33

STEWARD-1563

FERMILAB
MAY 10 2000
LIBRARY

PREPRINTS of the STEWARD OBSERVATORY

THE UNIVERSITY OF ARIZONA
TUCSON, ARIZONA 85721- 0065 U.S.A.

No. 1563

Fermilab Library
0 1160 0091197 8

KINEMATICS, KINETIC TEMPERATURES AND COLUMN DENSITIES OF NH_3 IN THE ORION HOT CORE

T.L. WILSON[1,2], R.A. GAUME[3], P. GENSHEIMER[1], K.J. JOHNSTON[3]

NAME	I.D No.	M.S.

ACCEPTED BY THE ASTROPHYSICAL JOURNAL

[1]Sub-Millimeter Telescope Observatory, Steward Observatory, The University of Arizona, Tucson, AZ 85721
[2]Max Planck Institut für Radioastronomie, Postfach 2024, D-53010 Bonn, Germany
[3]U.S. Naval Observatory, 3450 Massachusetts Ave., NW, Washington, DC 20392-5420

Kinematics, Kinetic Temperatures and Column Densities of NH_3 in the Orion Hot Core

T. L. Wilson[1,2], R. A. Gaume[3], P. Gensheimer[1], K. J. Johnston[3]

Received _____; accepted _____

[1]Sub-Millimeter Telescope Observatory, Steward Observatory, The University of Arizona, Tucson, Az., 85721

[2]Max Planck Institut für Radioastronomie, Postfach 2024, D-53010 Bonn, Germany

[3]U.S. Naval Observatory, 3450 Massachusetts Ave., NW, Washington, DC 20392-5420

ABSTRACT

Using the VLA, we have mapped the Orion Hot Core region (full extent 10″) with an angular resolution of $\sim 1''$ in the (J,K)=(4,4) and (10,9) inversion transitions of $^{14}NH_3$ and an angular resolution of 4″ in the (J,K)=(2,2) and (3,3) inversion transitions of $^{15}NH_3$. All of the single-dish flux density for the (10,9) transition was recovered by the VLA, but a substantial fraction of the flux density in the (4,4) and $^{15}NH_3$ (3,3) lines was not detected. The missing flux density is from the spatially extended 'spike' component. Assuming that local thermodynamic equilibrium (LTE) holds, we have calculated the optical depths of the (4,4) inversion transition for all positions where the main and satellite lines were detected with sufficient signal-to-noise ratio. We combined our (10,9) data with these (4,4) line results to produce images of the rotational temperature, T_{rot}, and the column density of ammonia, $N(NH_3)$. For the H_2 densities in the Hot Core, $T_{rot}= T_{kin}$, the kinetic temperature. An additional determination of T_{kin} and $N(NH_3)$ was made by combining our (10,9) inversion line data with our $^{15}NH_3$ (3,3) inversion line results. The $^{15}NH_3$ inversion transitions have no quadrupole hyperfine structure so that the line shapes are simpler. The moment distribution of the $^{15}NH_3$ (3,3) line shows that the largest intensity- weighted line width arises close to the center of the Hot Core region. Thus we may have discovered a low luminosity outflow source embedded in the Hot Core. Alternatively, this may be a result of gas motions related to source 'I', which is about half a beamwidth from this feature.

Subject headings: ISM: molecules, ISM: protostars, ISM: radio lines

1. Introduction

The 10″ (equivalent to 0.02 pc at 500 pc) diameter Hot Core source in the Orion KL region contains a high abundance of complex species, such as CH_3CH_2CN. This source has been the subject of a large number of high angular resolution molecular line studies in the radio wavelength range (see, e.g., Blake et al. 1996, Wright, Plambeck & Willner 1996). In single-dish spectra, there are normally three blended components: (1) a 'spike' feature formed in a spatially extended region with $T_{kin} \approx 55$ K and a narrow Full Width to Half Power (FWHP) line width, (2) a 'Plateau' component from a fairly compact region with a wider line width, and (3) a Hot Core component which we discuss next. From multi-line studies of inversion transitions ((J,K) $\rightarrow$ (J,K)) of the $^{14}NH_3$ molecule, Hermsen et al. (1988b) estimated that the Hot Core has an average H_2 density, $n(H_2)$, of $\sim 10^7$ cm^{-3} and an average kinetic temperature, T_{kin}, of 165 $\pm$ 5 K. Later studies of higher lying metastable (J=K) inversion transitions showed the presence of another component with T_{kin}=400$\pm$40 K (Wilson et al. 1993). The range of T_{kin} obtained from NH_3, 165 K to 400 K, form upper and lower bounds to values estimated from other species, such as ^{13}CO (Genzel, Poglitsch & Stacey 1988), HDO (Petuchowski & Bennett 1988), CH_3CN (Wilner, Wright & Plambeck 1994) and HC_3N (Goldsmith, Krotkov & Snell 1985, Wright et al. 1996). In the following we will not explicitly give the atomic weight of the normal isotopic species.

The Hot Core region also contains a number of near infrared sources and H_2O masers (see Gaume et al. 1998 for an overlay). Since the Hot Core is located in the Orion Molecular Cloud, where O and B star formation is active, it is likely that at least some of the near–IR maxima (Stolovy et al. 1998) are embedded stars which affect the gas. Downes et al. (1981) and Wynn-Williams et al. (1984) had proposed that the only significant heating source is the heavily extincted 2 μm emitter IRc2, which they argued was also an SiO maser and the source of the energetic CO outflow. The initial measurements of the SiO maser had angular

resolutions of a few arc seconds (Welch et al. 1981). Later measurements had improved sensitivity but the angular resolutions were still too low to investigate the structure in detail (Barvinis 1984, Morita et al. 1992, Wright et al. 1995, Baudry, Herpin & Lucas 1998). Recent VLBI data show an outflow-like structure (Greenhill et al. 1998, Doeleman, Lonsdale & Pelkey 1999). From near-IR data, Dougados et al. (1993) resolved IRc2 into a number of regions, and Gezari (1992) has shown that the position of IRc2 is definitely separated from the position of the SiO maser. Extinction is very large in this region, even at 2μm; a recent spectroscopy study of near–IR reflected light was carried out by Morino et al. (1998). In contrast to the near–IR, radio emission is not affected by extinction. From radio continuum data, Menten & Reid (1995) have shown that there are at least 3 radio continuum sources in the IRc2 region. They showed that the most intense radio source, 'I', is coincident with the SiO maser source and have argued that 'I' is the most luminous continuum source in the IRc2 region. On an angular scale of $5''$, Hermsen, Wilson & Bieging (1988a) had argued that *at least* two heating sources are required to explain the peak NH_3 line temperatures found in the Hot Core: One in the northern part of the Hot Core, presumably source 'I', with another in the southern part of the Hot Core.

Although there have been a large number of radio continuum and IR maps of the Hot Core, the interaction of heating sources and molecular gas is still an open topic, since there have been no determinations of T_{kin} of the molecular gas on a $\sim 1''$ scale. Maps of maser lines *cannot* be used to accurately determine T_{kin}, since the influence of excitation and line optical depth are very uncertain (see, e.g., Johnston et al. 1997). Thus, measurements of thermal line radiation are needed; however, a determination of T_{kin} from a comparison of *different* species (see, e.g., Blake et al. 1996) is suggestive but not conclusive, since interstellar chemistry will usually cause different species to have somewhat different spatial distributions. To determine the spatial distribution of T_{kin}, one must produce molecular line images of different transitions of a single molecular species. To insure accurate calibrations,

the same telescope and receiver system should be used to measure all of the lines. The T_{kin} values found for the Hot Core range from ~100K to ~600K. To estimate T_{kin} in this range, one must have measurements of transitions between levels which are between 120K and 1200K above the ground state. We have chosen to employ the NH_3 molecule because: (1) the inversion line data allow an accurate estimate of the kinetic temperature and (2) many of the inversion lines lie within the analyzing band of the 1.3 cm system of the VLA telescope of the NRAO[4]. For details of the properties of the NH_3 molecule, see Rohlfs & Wilson (1996) or Townes & Schawlow (1975). Most crucial is the choice of the inversion line transition from energy levels ~1000K above the ground state, since these transitions are rather weak (see, e.g., Wilson et al. 1993). The (J,K)=(10,9) transition of ortho-NH_3 is the most intense line above 1000 K above ground which is in the tuning range of the VLA. This was measured to have a peak line flux density of 0.5 Jy (see, e.g., the NH_3 inversion line data collected in Hermsen et al. 1988b). Metastable transitions (i.e. those with J=K) are known to be collisionally excited (see Rohlfs & Wilson 1996). Thus the ratio of metastable NH_3 transitions can be used to determine T_{kin}. The (10,9) transition is not metastable. However, the data of Hermsen et al. (1988b) showed that the population of the (10,9) levels are directly related by the kinetic temperature to the population of the (9,9) levels. In addition to the (10,9) inversion line, we have imaged the (4,4) metastable (J=K) transition of para- NH_3 and also the rarer isotope $^{15}NH_3$ in the (2,2) inversion line of para-NH_3 and the (3,3) inversion line of ortho-NH_3. The (4,4) levels are ~200K above the ground state, while the (3,3) levels are 120K and the (2,2) levels are 64K above ground. The (4,4) inversion line of NH_3 is optically thick; the ratio of satellite to main groups of hyperfine components are in LTE. From these ratios, it is possible to determine the optical

[4]The National Radio Astronomy Observatory is a facility of the National Science Foundation operated under cooperative agreement by Associated Universities, Inc.

depths of the main group of hyperfine components. By combining the optical depths and peak line intensities, we can determine the column densities in the (4,4) levels. The (10,9) line is optically thin, so the integrated line intensities are directly related to the column densities. The rotational and kinetic temperatures are related to the ratios of these column densities.

From the solar system $N/^{15}N$ ratio, 270 (see Wilson & Rood 1994), and the NH_3 optical depths measured for Orion KL (see, e.g. Hermsen et al. 1988b), the $^{15}NH_3$ inversion lines are optically thin. In addition, $^{15}NH_3$ has no quadrupole hyperfine structure, so our $^{15}NH_3$ data provide images of the kinematics unaffected by line optical depth and quadrupole structure. Using the $N/^{15}N$ ratio, we have obtained an additional estimate of T_{kin} and column density on an angular scale of 4″.

2. Observations

We measured the (J,K)=(10,9) non-metastable transition of ortho-NH_3, at 24205.287 MHz and the metastable (4,4) transition of para-NH_3, at 24139.417 MHz. These data were taken in 1993 July 30 with the VLA in the C configuration. Approximately 4.5 hr of the 7 hr run were spent observing the NH_3 transitions, the remainder of the time was dedicated to primary flux calibration (using 3C286, with a flux density of 2.4 Jy in 1993), bandpass calibration (using 3C84), and phase calibration (using 0539-057, with a flux density of 1.049 Jy). The observations were conducted in a 2 IF spectral line mode; each IF was tuned to observe one of the two NH_3 transitions. Each IF consisted of sixty-four 97.656 kHz channels; channel 32 of the 64 was tuned to an LSR velocity of 8 km s^{-1}. The channel separation used was 97.6 kHz (=1.2 km s^{-1} at the line frequency). The data were processed both with and without Hanning weighting of the line channels; the latter producing a velocity resolution 1.2 times the channel separation, the former 2 times the channel separation.

Measurements of the (J,K)=(2,2) and (3,3) metastable inversion transitions of $^{15}NH_3$ at 22649.843 MHz and 22789.421 MHz were made 1996 August 20 in a 7.5 hour period while the VLA was in the D configuration. The observing procedures were similar to that used in our 1993 July 30 measurements, with the exception that 3C48 was used for primary flux calibration; we assumed that the flux density of this source was 1.14 Jy at the time of the observations. From this measurement, the flux density of 0539-057 was determined to be 0.755 Jy; this source was used to calibrate the line intensities. In addition, telescope pointing corrections were determined and applied to the observations, using the reference pointing mode.

Both data sets were calibrated and imaged using the AIPS software package of the NRAO. Images with both uniform and natural weighting were made from the u, v data for the (4,4) and (10,9) lines. For the $^{15}NH_3$ data, we used only uniform weighting which produces an image with higher angular resolution; this is needed to reach a resolution closer to that of the (4,4) and (10,9) line data. The resultant spatial resolution and rms noise of individual channel images varied depending on the specific parameters chosen for the Fourier transform step (u,v, and channel weighting). In the frequency domain we chose to use normal spectral weighting, that is, the data are not Hanning smoothed. These choices gave the angular resolutions, velocity resolutions and sensitivities summarized in Table 1.

3. Results

3.1. Comparison with single dish results

In Fig. 1 we show a comparison of our VLA results with 100m data. For this comparison, we have summed the VLA data over the Hot Core. For the (4,4) inversion line data, the VLA has recorded 51% of the *peak* single dish flux density (from Hermsen et

al. 1988b). There is also a marked difference in the line shapes measured with the VLA and 100m telescopes. There is a ridge component extended over minutes of arc, at $V_{lsr} \approx 8.0$ km s^{-1}. Emission from this component has not been detected by the VLA. Our comparison in Fig. 1 shows that *none* of the single dish flux density from the 'spike' component has been detected by the VLA. If we compare the single dish flux density at the velocity of the peak of the profile measured with the VLA, we find that *all* of the emission from the Hot Core is recorded by the VLA. The uncertainties in the 100m data are large for the (10,9) line (taken by Ziurys et al. 1981). To within the errors, the VLA has recorded all of the single dish peak flux density. For the (3,3) inversion line of $^{15}NH_3$, the VLA has recorded 60% of the single dish peak flux density (from Hermsen et al. 1985). There are two velocity components corresponding to the Hot Core and to the spike component, in both the single dish and VLA data. As measured with the VLA, the radial velocity of the peak line emission in the $^{15}NH_3$ (3,3) line is 7.5 km s^{-1}, while emission in the highly excited (10,9) inversion line and the (4,4) line peaks at 5.5 km s^{-1}. The red shift of the $^{15}NH_3$ data is partly due to the presence of the spike component. The (3,3) line arises from energy levels 120K above ground, the emission could arise from more extended, lower density ridge gas. In contrast, the (10,9) line arises from levels $\geq$1000K above ground, so requires the more extreme conditions present only in the Hot Core. However, our images of the $^{15}NH_3$ (3,3) line (Fig. 3) show the same shape as in the (4,4) emission, so the VLA is measuring Hot Core gas. The difference in radial velocity could be caused by excitation, line optical depth effects or indicate an uncertainty in the rest frequency.

Our VLA (4,4) line data do not contain a measurable contribution from the 'spike' component. This lack of response of the VLA simplifies comparisons of (4,4) with (10,9) results, or with the $^{15}NH_3$ (3,3) line data. Although the 'spike' component has been eliminated, the 'Plateau' component (FWHP of $\sim$25 km s^{-1}) may be present in the VLA results for the (4,4) line. Since the total analyzing bandwidth we used is too narrow to fully

include the Plateau feature, and since there are sizeable hyperfine satellite components at ± 23.9 km s^{-1} and ± 30.9 km s^{-1} from the main line, the Plateau would appear as a zero offset in our spectrometer band. The 'Plateau' component is definitely *not* present in our (10,9) or $^{15}NH_3$ spectra. The differences between the (4,4) and (10,9) spectra are caused by excitation and optical depth effects. Then there may be two features contributing to the (4,4) data, the 'Plateau' and 'Hot Core' but only one, the 'Hot Core' in the (10,9) spectrum. This difference might cause the rotational temperature calculated from the ratio of column densities of (10,9) and (4,4) data to be biased toward lower values.

A number of authors have speculated that NH_3 lines emitted from the Hot Core had flat-topped line shapes because of the large optical depths. The VLA (4,4) profile in Fig. 1 has a large optical depth, but a gaussian shape. Most likely, this emission arises from a large number of clumps each with a large optical depth; what we measure is the velocity distribution of the ensemble of clumps. This must have a gaussian distribution. The spectra at each position are rather noisy, but show hints of flat-topped profiles, as found by Pauls et al. (1983).

3.2. Images of Individual Channel Maps

We show contour plots of a few selected velocity channels from our (4,4) and (10,9) inversion line data in Fig. 2. We have chosen radial velocities close to the peak of the Hot Core emission. As found previously, for radial velocities more positive than 10 km s^{-1}, there is an additional component of molecular line $\sim 6''$ East-NE of IRc2. For the more blue-shifted velocities in Fig. 2, many of the NH_3 clumps are centered near, but SE of the continuum sources I, n, and IRc2. We show the location of these sources as crosses in Fig. 2. For the velocities shown, the NH_3 emission is located in a NE-SW ridge which is $1''$ to $2''$ SE of source 'I'. Besides this ridge of NH_3 emission, at mid to extreme red shifted velocities

there is a second NH_3 component centered near IRc6.

For the (10,9) emission, the most blue-shifted velocities are centered on 'I', 'n' and IRc7. From Fig. 2, the NE-SW ridge actually bends around 'I' in the red shifted velocities. This is seen particularly well in the 5.6 km s^{-1} channel. Emission clumps are found toward sources 'n', IRc7 and IRc6. In individual velocity channels, the emission curves around, and actually avoids the position of source 'I'.

The extent of the (10,9) line emission is much more compact than that of the (4,4) line emission. Since the (10,9) levels can be populated only at high T_{kin}, a qualitative comparison of these images shows that the hottest NH_3 is located in the NE part of the Hot Core. A quantitative estimate of T_{kin} is given in Section 4.1. Even though the hottest gas is close to source 'I', there is *little* NH_3 toward the location of 'I' itself.

3.3. Images of $^{15}NH_3$ Emission

In Fig. 3, we present our map of the ortho-$^{15}NH_3$ (3,3) inversion line data. The results for the (2,2) line of para-$^{15}NH_3$ are the same, but the signal to noise ratio is lower because the ortho species has a larger statistical weight. In Fig. 3(a) we show the zeroth moment or total integrated intensity, in Fig. 3(b), the first moment, or intensity-weighted radial velocity, and in Fig. 3(c) the second moment, which is the intensity-weighted line width of $^{15}NH_3$ (3,3) data. (For a gaussian line profile the second moment is a factor of 2.35 less than the gaussian FWHP). These data are an important extension of our (4,4) and (10,9) results, since the line optical depths are much smaller and the $^{15}NH_3$ spectra have no quadrupole hyperfine structure. These factors allow a simpler interpretation of radial velocities and line widths. However, the small intensities prevent us from reaching a high signal-to-noise ratio, although these weak signal levels insure that the $^{15}NH_3$ emission is optically thin.

In order to reach a reasonable signal-to-noise ratio, we have taken these data in the most compact configuration of the VLA; these results have a ~4 times lower spatial resolution in one dimension (or a factor of 14 lower in area) than our (4,4) and (10,9) line data.

Our $^{15}NH_3$ integrated emission (Fig. 3(a)) is relatively weaker in the NW than the image of NH_3. This indicates that the optical depth in the (3,3) line of NH_3 is smaller in the NW. As will be shown in Section 4.2, the T_{kin} is also smaller in the NW, so the total column density of NH_3 must be smaller there. In the rest of the Hot Core, there is good agreement in overall shape and radial velocities between the $^{15}NH_3$ (3,3) data and the VLA results for the (3,3) inversion of NH_3 (Pauls et al. 1983), as well as our (4,4) results (next section).

The radial velocities are bluer by 0.5 km s^{-1} in the NE part of the Hot Core. This is consistent with the hypothesis that most of the NH_3 is in front of outflow sources and being pushed in our direction. This foreground material causes the large near–IR extinction estimated for IRc2. Since the NH_3/H_2 ratio varies by a factor of 100 from source-to-source (see van Dishoeck et al. 1993), our data cannot be used to obtain an extinction estimate.

The most interesting result is that the second moment, which is the intensity-weighted line width, shows that the *largest* value does *not* occur at or near the position of sources 'I' or 'n', rather at a location ~2″ to the south of these sources. This is only one-half a beamwidth from source 'I'. There is no IR source at this position. This wider line width may be related to the CO outflow (see, e.g., Rodríguez-Franco, Martín-Pintado & Wilson 1999), to gas motions related to source 'I', which is about half a beamwidth to the NE, or to another outflow. Since the radial velocity of this $^{15}NH_3$ (3,3) feature is that of the Hot Core, this is embedded in the Hot Core itself. This feature may have been the 'zero offset' in the NH_3 (3,3) line images of Pauls et al. (1983). Since the NH_3 Hot Core line optical depth was large, the 'zero offset' will be confused with the hyperfine satellites of the (3,3)

line of NH_3, which are separated by ± 21.2 and ± 29.1 km s^{-1} from the main group of hyperfine components. The Full Width to Zero Power (FWZP) of this feature is $\sim$20 km s^{-1}, so if this were an outflow, it is much less energetic than the CO outflow, which reaches a FWZP of $\sim$100 km s^{-1}. From the radial velocity and position, it is possible that this feature is an outflow from another star embedded *in* the Hot Core itself.

4. Kinetic Temperature and Total NH_3 Column Density Images

4.1. Kinetic Temperature

From Fig. 2, the (10,9) emission is more compact than the (4,4) emission and is concentrated to the NE part of the Hot Core. We interpret this as a gradient in $T_{rot}=T_{kin}$. The warmest NH_3 is found where the (10,9) emission is found; the largest heat input to the Hot Core is from the NE.

For a detailed investigation of the distribution of T_{kin}, we have combined the (4,4) inversion line results with the (10,9) data. We assume that the inversion transitions are thermalized. From a least-squares fit to 28 inversion-rotation lines of NH_3, Hermsen et al. (1988b) showed that all of these NH_3 lines are thermalized at a temperature of 165 K. If optically thick, the peak line intensity of the (10,9) emission would be $\sim$165 K; the measured peak line temperature is much smaller, so we can assume that the (10,9) inversion line is optically thin. Then the beam-averaged column density is proportional to integrated line intensity. The (4,4) line is known to be optically thick (see, e.g., Hermsen et al. 1988b), so a more complex analysis is needed. Deviations from LTE for such line ratios are rare (see Gaume et al. 1996), so we are justified in assuming that the excitation of the main and satellite lines is in LTE. Then from the ratio of hyperfine components, we can estimate the optical depths of the (4,4) line and column densities in the (4,4) energy levels. We have

determined the total column density in the (4,4) levels by using the average integrated intensities of the three groups of the hyperfine satellite components which were in the analyzing band of the VLA. The relation, adapted from Wilson, Downes & Bieging (1979), is

$$N_{u+l}(4,4) = 5.65\,10^{14} \int T_{sat} dv \tag{1}$$

where T_{sat} is the observed main beam brightness temperature of a hyperfine satellite. By an application of Eq. (1) for each position, we obtained the column densities of the (4,4) levels for a 3.9 km s^{-1} velocity interval. We applied a similar relation to the main group of hyperfine components of the (10,9) inversion transition. We have assumed that the (10,9) line is optically thin, in contrast to the (4,4) transition. We have obtained the (10,9) column densities from the integrated line intensities. Then we applied the Boltzmann relation to the ratio of these column densities. If we assume an ortho-to-para ratio of 2, we have

$$T_{kin} = -820/\left(\ln(0.233\frac{N(10,9)}{N(4,4)})\right) \tag{2}$$

The result is the image of T_{kin} shown in Fig. 4(a). A number of comments are in order. First, the missing flux density in the (4,4) line data arise from the 'spike' component, so do not bias the T_{kin} values. However, T_{kin} *is* sensitive to noise in the (10,9) line data. For this reason, we have set the cut-off at the 60 mJy· km s^{-1} $beam^{-1}$ level, far above the RMS noise. Taking lower cut-off values increases the noise in the T_{kin} image, but does not significantly change the image. The dynamic range in T_{kin} is determined by the choice of NH_3 inversion lines, in the sense that the (4,4) line arises from energy levels 200 K above ground. Thus, there is little sensitivity to gas with $T_{kin} \leq$ 50 K. The image shows only small variations in T_{kin}. The extent of NH_3 with $T_{rot} \geq$ 130K is close to the extent of the (10,9) line. The highest values of T_{kin} occur for positions near to, but offset from, the

cluster of sources 'I' and 'n'. From our images of individual channels in Fig. 2, the NH_3 emission avoids the position of source 'I'. Taking the ratio of two such images gives a result which is more extended than either. Although there *seems* to be T_{kin} information at the position of source 'I', this is not reliable. Our data are consistent with the conclusion of Menten & Reid (1995) that 'I' is a very luminous source. Close to 'I', the NH_3 may be dissociated by photons or by shock waves. The extinction toward 'I' is larger than 100 visual magnitudes (see, e.g., Menten & Reid 1995). Thus, if photons were the only dissociating agent, there should be *some* NH_3 along the line of sight. The combination of shocks and a harsh ultraviolet environment would insure that there are no fragile molecules such as NH_3 (dissociation energy 4 eV) near source 'I'. However, unless the line-of-sight geometry is very peculiar, the very slow decline of T_{kin} as a function of positional offset from source 'I' indicates that source 'I' is *not* the *only* source providing significant heat input to the Hot Core.

In addition to the (4,4) emission shown in Fig. 2, there is emission in the NW part of the Hot Core, with radial velocities in the range 10 to 12 km s^{-1}. In the NW, we have searched this velocity range and find that the optical depth of the main group of hyperfine components of the (4,4) inversion line can be as large as 40. The largest column density in the (4,4) inversion line is $10^{17}cm^{-2}$. When we combine the limit for the column density in the (10,9) inversion line with the (4,4) inversion line column density data, we find that the value of T_{kin} is $\leq$120K. The actual value of T_{kin} may be lower. Our estimate is limited by RMS noise in the (10,9) image at this position. Increased sensitivity would allow a larger dynamic range in T_{kin}. However, from Eq. 2, T_{kin} depends on the logarithm of the column density ratio. Thus, a substantial increase in sensitivity is needed to lower our limit by more than 30K.

We have obtained an additional, independent determination of the T_{kin} distribution by

combining the $^{15}NH_3$(3,3) inversion line data with the $^{14}NH_3$ (10,9) inversion line data. In this analysis, we need to make no assumptions about the ortho-to-para ratio, since both transitions arise from ortho-NH_3. However, we must assume that the $^{14}N/^{15}N$ ratio is the solar system ratio, 270. In addition, we spatially smoothed the (10,9) data to the 4″ angular resolution of the $^{15}NH_3$ (3,3) inversion line data. The distributions of T_{kin} from these two methods are similar but the T_{kin} values obtained from the combination of (10,9) and $^{15}NH_3$ (3,3) line data are, on average, 20K higher. There are three possible causes for this small difference in T_{kin}: (1) the $^{14}N/^{15}N$ ratio should be set 15% higher (2) that the ortho-to-para ratio should be reduced by this amount, or (3) there are differing amounts of missing flux density in the $^{15}NH_3$(3,3) inversion line data.

4.2. $^{14}NH_3$ Column Densities

If the NH_3 population is in LTE, we can obtain an image of the total column density, $N(NH_3)$, from the distribution of T_{kin} and column densities of the (4,4) line. From Rohlfs & Wilson (1996), there is a formalism to obtain the total population. Inserting the numerical values, the relation follows Rohlfs & Wilson (1996) Eq. 14.63:

$$N(\mathrm{NH_3}) = 0.046\, N(\mathrm{NH_3})\, \mathrm{T}^{3/2}\, \mathrm{e}^{200/\mathrm{T}} \tag{3}$$

where $T=T_{rot}=T_{kin}$; we have used an average value of 130 K for the whole map. We show the image of $N(NH_3)$ in Fig. 4(b); there is no large variation. Because the radial velocities used in our images are centered around 5.5 km s^{-1}, the NW part of the Hot Core, with a v_{LSR} of 13 km s^{-1}, is not included in this image. For the NW component, there is no emission in the (10,9) inversion line, and the optical depths of (4,4) line are smaller than the values measured from the center of the Hot Core. Our best estimate is that the total column density in the NW feature is a factor of 5 to 10 below the peak value shown in

Fig. 4(b).

4.3. $^{15}NH_3$ Column Densities

An additional determination of the total column density of NH_3 can be obtained from the $^{15}NH_3$ data, given a $^{15}N/^{14}N$ ratio and assumptions about the ratio of the total population to that in the (2,2) or (3,3) levels. We assume that: (1) the T_{rot} is equal to that found for the NH_3 and (2) the metastable (J=K) and those non- metastable levels which connect directly to the metastable levels (i.e., J+1=K) have LTE populations, but that no other energy levels of $^{15}NH_3$ are populated. The partition function for this case is given in the appendix of Pauls et al. (1983). Applying this, we find that the NH_3 column density in the center of the Hot Core is 4×10^{18} cm^{-2}. This is one-half of the estimate made by Pauls et al. (1983). There are significant uncertainties in the optical depths, temperature variations in the cloud, isotope ratios; in addition there may be deviations from LTE. Thus, factor-of-two difference between total column density estimates are reasonable.

5. Discussion

5.1. General Properties

Qualitatively, the NH_3 requiring the most extreme excitation is located in the NE part of the Hot Core, close to sources 'I' and 'n'. This gas has a velocity blue–shifted with respect to the average V_{lsr} of the Hot Core. These results lead us to conclude that: (1) sources 'I' and 'n' must play an important role in heating the NH_3, and (2) most of the NH_3 is located between the heating sources and the observer. In Fig. 5 we show a montage of the integrated emission in the (10,9) transition in the left panel, and the distribution of H_2O masers measured by Gaume et al. (1998) in the right panel. The SiO maser emission

is also associated with source 'I'. Together these show that 'I' is an unusual source.

Downes et al. (1981) and Wynn-Williams et al. (1984) had attempted to unify all energetic phenomena in Orion KL by assuming that one source gave rise to: (1) the SiO maser emission, (2) CO outflow and (3) also heated the Hot Core. Source 'I' definitely provides (1) and (3), and perhaps (2). On the basis of our high sensitivity maps, Rodríguez-Franco, Martín-Pintado and Wilson (1999) find that the outflowing CO with velocities ± 80 km s^{-1} from ambient is found $\sim 30''$ north of source 'I'. Rodríguez-Franco et al. (1999) have argued that the morphology of the velocity–position plots for the outflowing CO are consistent with a precessing jet. It is also possible that the outflow could be a very heavily obscured source north of source 'I'. At present, there seems to be little evidence for such a source.

5.2. Maximum Value of Kinetic Temperature

The maximum $T_{rot} = T_{kin}$ in Fig. 4(a) are only slightly lower than the value of 165 ± 5K obtained by Hermsen et al. (1988b) from a fit to both metastable and non-metastable inversion lines from energy levels up to 1000K above the ground state of NH_3. However, our values are significantly lower than the $\sim$400K value found by Wilson et al. (1993) from a fit to the intensities of six metastable inversion transitions arising from energy levels from 1000K to 2000K above the NH_3 ground state. Apparently, the 165K gas contributes to most of the column density in the (10,9) line. For reference, we show the plot of NH_3 column density for a given inversion transition versus energy of the levels involved in that transition in Fig. 6.

Given two transitions, we can reconcile our results in Fig. 4(b) with a simple two zone model. The cooler gas would have T_{kin}=130K, while the hotter gas has T_{kin}=400K. The

column density of the very hottest gas is only a few % of the column density of NH_3 we measure in the (4,4) transition (see Fig. 6). A specific model would be an 'onion-skin' arrangement. If we assume that 99.3% of the (4,4) level population and one-half of the (10,9) level population are in the outer, cooler region, we place the remaining 0.7% of the (4,4) level population and the remaining 1/2 of the (10,9) level population in an inner, hotter core. With this arrangement, we obtain agreement with the single dish results. It would be of great interest to image transitions such as the (14,14) which can arise only in the hottest gas, to test our model.

From an analysis of different K components of CH_3CN, Wilner et al. (1994) obtain a kinetic temperature of ~250 K in the Hot Core. However, since the highest energy level used in this analysis is only 128 K above ground, this value may not be very accurate. It is interesting that the maximum of the emission from the most highly excited energy level of CH_3CN is very close to our peak in the (10,9) line of NH_3. It is possible that closer to the heating source, species such as CH_3CN and NH_3 are destroyed.

5.3. Number of Heating Sources

The fact which supports our claim that there are at least two sources heating the Hot Core is the slow decline in the value of T_{kin} from the position of Source 'I'. If we assume that 'I' is the *only* significant heating source, and that the geometry of the NH_3-containing gas is not peculiar, then from the Stefan-Boltzmann law we expect a fall off in T_{kin} proportional to $R^{-0.5}$, where R is the distance from source 'I'. The fall-off is definitely slower, so ther must be other heating sources.

The local maximum in the spatial distribution of the $^{15}NH_3$ line width is coincident with the center of the Hot Core, but offset from any single near–IR source. However, this

is not evidence for an additional embedded source since this increased line width may be related to the highly energetic CO outflow.

There is some support from theory for the presence of a number of heating sources. Kaufman et al. (1998) have modeled the heating of the Hot Core, based on a symmetric cloud geometry. They concluded that there must be internal heating sources in the Hot Core itself. Source 'I' is external to the Hot Core, since this source is slightly north of the densest concentration of NH_3 which avoids the position of source 'I'. We surmise that close to source 'I', the NH_3 has been destroyed, and the dust has been removed. The peak T_{kin}, estimated from our data, is $\sim$170K. However, lower luminosity sources embedded in the Hot Core would be more effective in heating fragile species, since these can exist close to the heating source.

5.4. Classification of the Heating Sources

The mass or spectral type of *any* of the heating sources in the Orion KL or Hot Core regions is uncertain. Since the work of Kaifu, Buhl & Snyder (1975), there has been a discussion whether IRc2 is a 'protostar' or Red Giant star. It is possible that sources 'I' and 'n' are at very different line-of-sight distances from the NH_3. This seems unlikely, however. Then the fact that the NH_3 avoids the region close to source 'I', but not source 'n', is evidence that source 'n' has a lower effective temperature than source 'I'. Because the Hot Core region is crowded with IR sources, an accurate estimate of the luminosity is difficult. Wynn-Williams et al. (1984) had argued for a luminosity of 10^5 $L_\odot$. However, as noted by Menten & Reid (1995), the uncertainty in the luminosity could be a factor of 10. Morino et al. (1998) have carried out near-IR spectroscopy of the IRc2 region and report an effective temperature of 4500K, based on K' band studies of reflected light. These data were integrated over a 10″ region; because of the complexity an high extinction of the region,

this value of T_{eff} must be considered rather uncertain. If T_{eff} were so low, it is surprising that there is an HII region associated with source 'I' and extending to source 'n' (see the data of Chandler & Wood 1997). If however correct, this T_{eff} requires a source size of $\geq$100 A.U. to provide a luminosity of $\geq 10^4$ $L_\odot$. Morino et al. (1998) have collected arguments that this source is a 'protostar' (more correctly a young star) rather than a late–type red giant star; because of the large extinction in the infrared the uncertainties in luminosity are very large, and hence the argument of Morino et al. (1998) cannot be conclusive.

The larger line width found in $^{15}NH_3$ may be caused by an embedded outflow source rather than related to source 'I' or the CO outflow. If so, this source is *very different* from 'I', since it seems to have a small luminosity. We can estimate the mechanical luminosity of this source from our $^{15}NH_3$ data, and a number of assumptions. From Fig. 3, the excess linewidth at the center of the Hot Core is 2 km s^{-1}. The average line intensity in the outflowing gas is 1 K. From formulae similar to Eq. 1, we obtain a beam-averaged column density of 1.6 10^{14} cm^{-2}. Assuming that only metastable levels are populated, that the $N/^{15}N$ ratio is 270 and that the H_2/NH_3 ratio is 10^5, we find an H_2 column density of 4 10^{21} cm^{-2}. Summing over an area corresponding to the 4″ beam, we obtain a mass in the outflow of 10^{-3} $M_\odot$. The mechanical energy in the outflow is 4 10^{40} ergs. If the gas has been outflowing for 10^3 years, the mechanical luminosity is 3 10^{-4} $L_\odot$. From radial velocity and position, the $^{15}NH_3$ outflow can compress and heat gas in the center of the Hot Core. This source *does not* have a large influence on the dynamics of the high velocity outflow, but may influence the chemistry of the Hot Core.

5.5. Comparison with Other Molecular Line Images

The chemistry in the Orion KL nebula and the Hot Core region is very complex (see the images of Wright et al. 1996 and Blake et al. 1996). Different species have slightly different

spatial locations. This is caused by the formation and destruction mechanisms. The H_2O shell masers and the SiO masers are located on a line which is roughly perpendicular to the high velocity CO outflow (Gaume et al. 1998, Greenhill et al. 1998). However the centroid of the red and blue lobes of the CO outflow is about 6″ north of the position of source 'I'. Non-masering SiO emission is also located north of source 'I', but only 1″ north, not nearly as far north as the CO outflow. According to Chernin & Wright (1996), the CO outflow may be deflected by the Hot Core. The most complex species, such as ethyl cyanide, are centered about 1.5″ south and 1″ east of source 'I'. The vibrationally excited HC_3N emission is close to the center of ethyl cyanide emission, but slightly closer to source 'I'. The distribution of HDO emission is very similar to that of the (10,9) emission from NH_3. It is possible that the complex species in the eastern part of the Hot Core are located where the low velocity outflow in $^{15}NH_3$ intersects a region of dense gas heated by source 'I'. Closer to 'I', dust has been ablated and only molecules such SiO can survive. The H_2O masers are found close to source 'I' must be formed in a post-shock region where H_2O can be readily formed. According to Wright et al. (1996) there are two zones of different chemistry, at larger scales. The first is a region where SO and SO_2 are formed from the collision of stationary gas with an energetic outflow. At larger distances, one finds HCN and HC_3N which traces material freed from clumps at the edges of a cavity evacuated by the high velocity outflow.

6. Summary

From an analysis of our VLA images of the (J,K)=(4,4) and (10,9) inversion transitions of $^{14}NH_3$ and our image of the (3,3) inversion transition of $^{15}NH_3$, we conclude that:

1. There are $\sim$ 10% variations in the measured value of T_{kin}, with the highest values of T_{rot}=T_{kin}=170K are in the NE part of the Hot Core. The highest column density and

hottest NH_3 are found in a NE-SW ridge 1″ to the east of source 'I'. The warmest gas has a blue shift of ~1 km s^{-1} relative to the average velocity of the Hot Core. Since the inversion lines used for this study are all >120K above ground, our images pick out warmer gas.

2. The Column Densities of NH_3 have been determined on a position-by-position basis. The maximum values of column density agree to within a factor of two with that of previous NH_3 results, which were based on a single inversion line.

3. In previous publications, radio source 'I' was identified as the dominant heating source of the Hot Core. Our data show that several other components also contribute significantly to the excitation of the hot core: source 'n', IRc7, and IRc6. The ridge NH_3 avoids the position of source 'I'. Either shock waves or ionizing flux from these radio sources probably destroys the nearby NH_3.

4. Our $^{15}NH_3$ images show that emission with the largest line widths are near the position of sources IRc7 and 'n'. This may be caused by the presence of an embedded low velocity outflow source. If so, this source has a mechanical luminosity of 3 $times 10^{-4}$ $L_{\odot}$, if this source has an age of 10^3 years. Alternatively, the larger line width may be a result of gas motions related to source 'I', which has a position of half a beam width to the NE.

REFERENCES

Barvainis, R.E. 1984 ApJ 279, 358

Baudry, A., Herpin, F., Lucas, R. 1998 A & A 335, 654

Blake, G.A., Mundy, L.G., Carlstrom, J.E., Padin, S., Scott, S.L., Scoville, N.Z., & Woody, D.P. 1996, ApJ 472, L49

Chandler, C., & Wood, D.O.S 1997, MN 287, 445

Chernin, L.M., & Wright, M.C.H. 1996, ApJ 467, 676

Dishoeck, E. van, Blake, G.A., Drain, B.T., Lunine, J.I. 1993 in 'Protostars and Planets III' ed. E.H. Levy, J.I. Lunine, The Univ. of Arizona Press, Tucson

Dougados, C., Lena, P., Ridgeway, S.T., Christou, J.C., Probst, R.G. 1993, ApJ 406, 112

Doeleman, S., Lonsdale, C.J., Pelkey S. 1999, ApJ 510, L55

Downes, D., Genzel, R., Becklin, E.E., Wynn-Williams, C.G. 1981, ApJ 244, 884

Gaume, R.A., Wilson, T.L., & Johnston, K.J. 1996, ApJ 457, L47

Gaume, R.A., Wilson, T.L., Vrba, F.J., Johnston, K.J. & Schmid-Burgk, J. 1998, ApJ 493, 940

Genzel, R., Poglitsch, A., & Stacey G.J. 1988 ApJ 333, L59

Gezari, D.Y., 1992, ApJ 396, L43

Goldsmith, P. F., Krotkov, R. & Snell, R. L. 1985, ApJ 299, 405

Greenhill, L., Gwinn, C.R., Schwartz, C., Moran, J.M. & Diamond, P.J. 1998, Nature 396, 650

Hermsen, W., Wilson, T.L., Walmsley, C.M., & Batrla, W. 1985, A & A 146, 134

Hermsen, W., Wilson, T.L. & Bieging, J.H. 1988a, A & A 201, 276

Hermsen, W., Wilson, T.L., Walmsley, C.M., & Henkel, C. 1988b, A & A 201, 285

Johnston, K. J., Gaume, R.A., Wilson, T.L., Nguyen, H.A. & Nedoluha, G. E. 1997, ApJ 490, 758

Kaifu, N., Buhl, D. & Snyder, L. E. 1975, ApJ 195, 359

Kaufman, M. J., Hollenbach, D.J., & Tielens, A.G.G.M. 1998, ApJ 497, 276

Menten, K.M. & Reid, M.J. 1995 ApJ 445, L157

Morita, K.-I., Hasegawa, T., Ukita, N., Okumura, S.K. & Ishiguro, M. 1992 PASJ 44, 373

Morino, J.-I., Yamashita, T., Hasegawa, T., & Nakano, T. 1998, Nature 393, 340

Pauls, T.A., Wilson, T.L., Bieging, J.H., & Martin, R.N. 1983, A & A 124, 23

Petuchowski, S.J., & Bennett, C.L. 1988 ApJ 326, 376

Rohlfs, K., & Wilson, T.L. 1996 'Tools of Radio Astronomy', Springer-Verlag, Heidelberg

Rodríguez-Franco, A., Martín-Pintado, J., Wilson, T.L. 1999 A & A 344, L57

Stolovy et al. 1998 ApJ 492, L151

Townes, C.H., & Schawlow, A. 1975 'Microwave Spectroscopy', Dover Publ., N.Y.

Welch, W.J., Wright, M.C.H., Plambeck, R.L. Bieging, J.H. & Baud, B. 1981 ApJ 245, L87

Wilner, D.J., Wright, M.C.H., & Plambeck, R.L. 1994 ApJ 422, 642

Wilson, T.L., Downes, D. & Bieging, J.H. 1979, A & A 71, 275

Wilson, T.L., Henkel, C., Huettemeister, S., Dahmen, G., Linhart, A., Lemme, C., & Schmid-Burgk J. 1993, A & A 276, L29

Wilson, T.L. & Rood, R.T. 1994, Ann. Rev. A & A 32, 191

Wright, M.C.H., Plambeck, R.L. & Wilner, D.J. 1996, ApJ 496, 216

Wright, M.C.H., Plambeck, R.L., Mundy, L.G. & Looney, L.W. 1995, ApJ 496, 216

Wynn-Williams, C.G., Genzel, R., Becklin, E.E. & Downes, D. 1984 ApJ 281, 172

Ziurys, L.M., Martin, R.N., Pauls, T.A. & Wilson, T.L. 1981 A & A 104, 288

This manuscript was prepared with the AAS LaTeX macros v4.0.

Fig. 1.— A comparison of profiles of three ammonia inversion transitions studied in this paper. In all cases, the 100-m spectra (taken with a 43″ beam) are displayed above in each panel, while the VLA spectra are shown below, as histograms. The velocity scale is with respect to the Local Standard of Rest. The intensity scales of the 100-m data and VLA are in Jy. The 100-m intensities are obtained using the relation 0.86 Jy is equivalent to 1 K main–beam brightness temperature. The VLA intensities are in Jy, from a sum over the Hot Core region. **(a)** This is a plot of the (J,K)=(4,4) transition of $^{14}NH_3$, with arrows showing the locations of the quadrupole hyperfine satellites. The spectrum is newly measured; the result is in agreement with the data shown by Hermsen et al. (1988b). In **(b)**, we show the (10,9) inversion transition of $^{14}NH_3$. The 100-m spectrum was taken from Ziurys et al. (1981). In **(c)**, we show profiles of the (3,3) transition of $^{15}NH_3$. The 100-m data were taken from Hermsen et al. (1985).

Fig. 2.— We show the images of sets of velocity channels. In the upper panels, we show the (4,4) inversion line data, while in the lower panels we show the corresponding velocity channels for the (10,9) inversion line data. The contours for the (4,4) data are 2, 3, 4, 5, 6, 7, 8, 9, and 10 times 8.23 mJy beam^{-1}. For the (10,9) data, the contours are 3, 4, 5, 6, 7, 8, 9, and 10 times 4.80 mJy beam^{-1}. The beam size is 1.3″ by 0.9″, position angle 9.6°; 4.80 mJy beam^{-1} corresponds to 8.7 K, main beam brightness temperature. (Sensitivities and velocity resolutions are given in Table 1).

Fig. 3.— Results for the (3,3) inversion line of $^{15}NH_3$, taken with an angular resolution of 3.5″ by 2.8″, positon angle 3.26°. Since $^{15}NH_3$ has not quadrupole hyperfine structure, line widths and radial velocities are easier to determine than with NH_3. **(a)** We plot the image of integrated intensity, in units of Jansky beam^{-1} × m sec^{-1}. To convert to K× km s^{-1}, multiply by 0.22. **(b)** The image of the first moment, that is, mean velocity weighted by intensity. There is a marked blue shift of the radial velocities toward the NE part of the Hot Core. **(c)** The second moment, or the intensity-weighted velocity dispersion. The most interesting result is that the widest lines are located at the center of the Hot Core.

Fig. 4.— **(a)** We show an image of the rotational temperature, T_{rot}, averaged over 4.36 km s^{-1} to 6.79 km s^{-1}. Since NH_3 lines in the Hot Core region have large optical depths, T_{rot} is very nearly equal to the kinetic temperature, T_{kin}. The contour levels are 130 K to 170 K by 10 K. Outside the region shown, the signal-to-noise ratio in either the (10,9) or (4,4) lines is too small to calculate T_{rot}. **(b)** We show an image of the logarithm of the total column density of NH_3, obtained under the assumption of LTE excitation, and using a T_{kin}=130 K. The contours in this image are from 15.1 to 17.1 by 0.4. There is a minimum 0.5″ SW of source 'I', another 1″ east of 'I'.

Fig. 5.— In the left panel we show an image of the integrated intensity of the (10,9) transition of NH_3, which marks the location of hot gas. In the right panel, we use crosses to mark the positions of the shell H_2O masers imaged by Gaume et al. (1998).

Fig. 6.— The plot of normalized column density (averaged over a 43″ beam) versus energy (in Kelvin) of the lower level involved in the transition (reproduced from Wilson et al. 1993). The open circles represent the metastable (J=K) transitions, while the crosses represent the non-metastable transitions (J>K). The transitions labeled are those relevant for this paper. The slope of the straight line is the inverse of the rotational temperature, T_{rot}. In the Orion KL nebula, $T_{rot}=T_{kin}$. The transitions from lower lying levels are fit by T_{rot} = 165K; the transitions from levels $\geq$ 1000K are fit by T_{kin}=400K.

Table 1. Observing Log

species	Transition	Observing Date	angular Resolution (″)	velocity Resolution (km s^{-1})	RMS noise (mJy $beam^{-1}$)
$^{14}NH_3$	(4,4)	30 July 93	1.3 × 0.9	1.3	7.9
$^{14}NH_3$	(10,9)	30 July 93	1.3 × 0.9	1.3	7.8
$^{15}NH_3$	(2,2)	20 Aug 96	3.5 × 2.8	1.3	10
$^{15}NH_3$	(3,3)	20 Aug 96	3.5 × 2.8	1.3	10

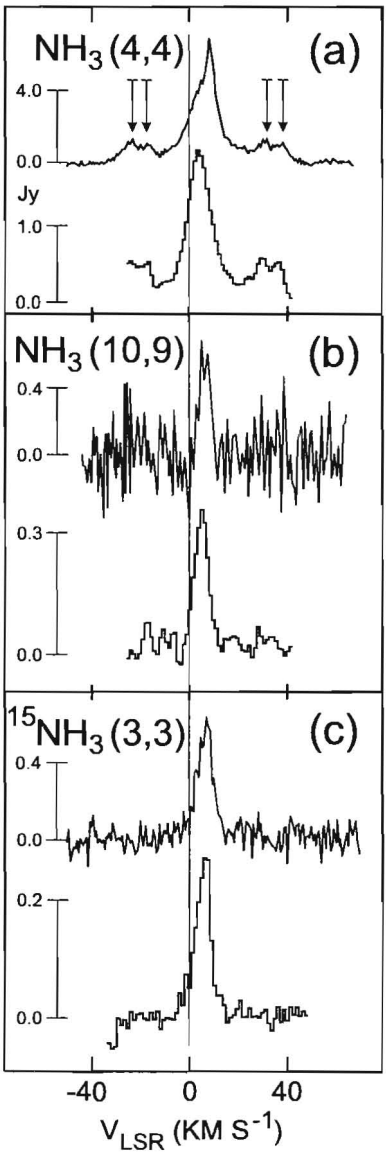
NH3 (4,4)
(a)
4.0
0.0
Jy
1.0
0.0
NH3 (10,9)
(b)
0.4
0.0
0.3
0.0
15NH3 (3,3)
(c)
0.4
0.0
0.2
0.0
-40
0
40
VLSR (KM S-1)

Fig. 1

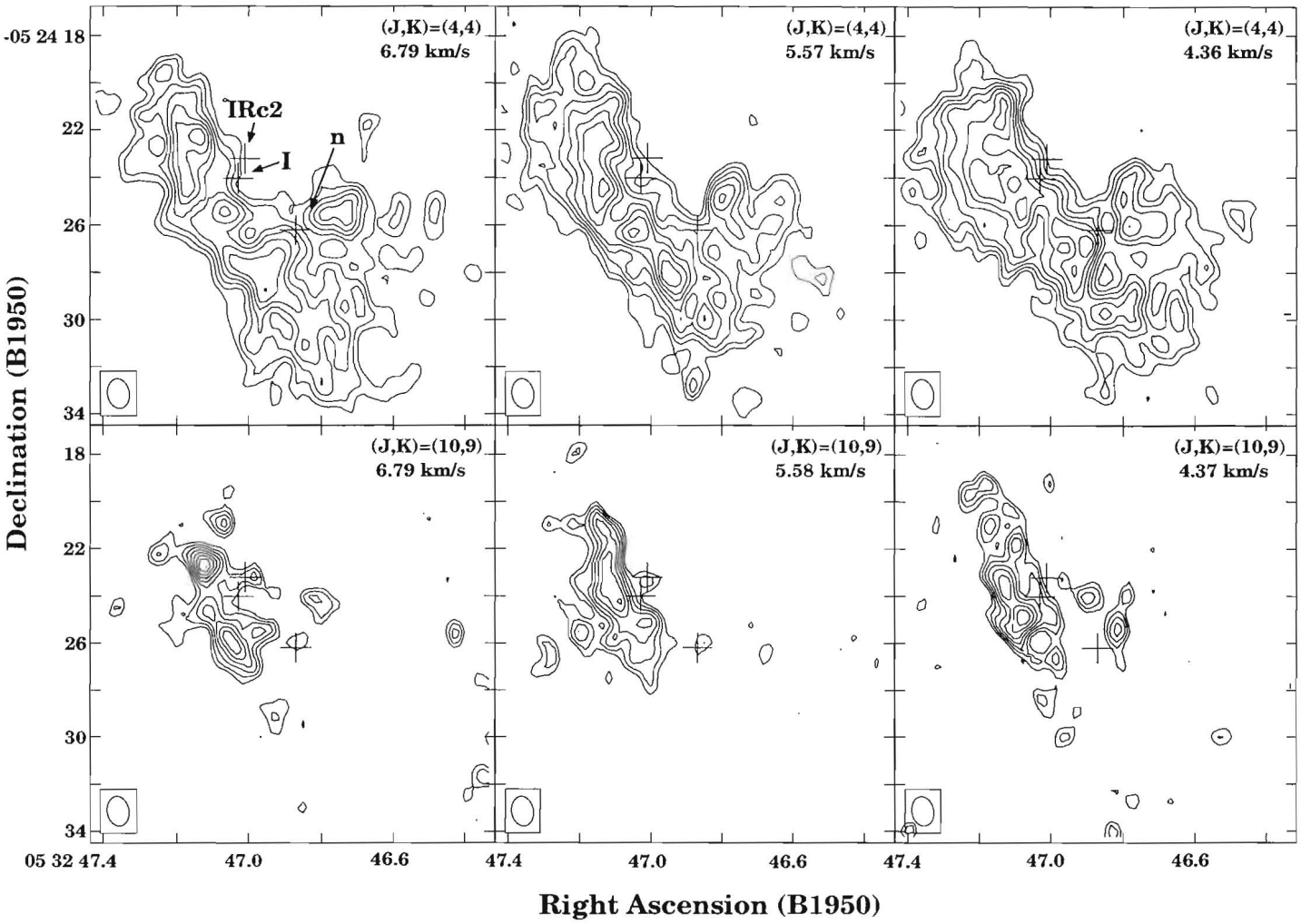
(J,K)=(4,4)
6.79 km/s
(J,K)=(4,4)
5.57 km/s
(J,K)=(4,4)
4.36 km/s
(J,K)=(10,9)
6.79 km/s
(J,K)=(10,9)
5.58 km/s
(J,K)=(10,9)
4.37 km/s
IRc2
I
n
-05 24 18
22
26
30
34
18
22
26
30
34
05 32 47.4
47.0
46.6
47.4
47.0
46.6
47.4
47.0
46.6
Declination (B1950)
Right Ascension (B1950)

Fig. 2

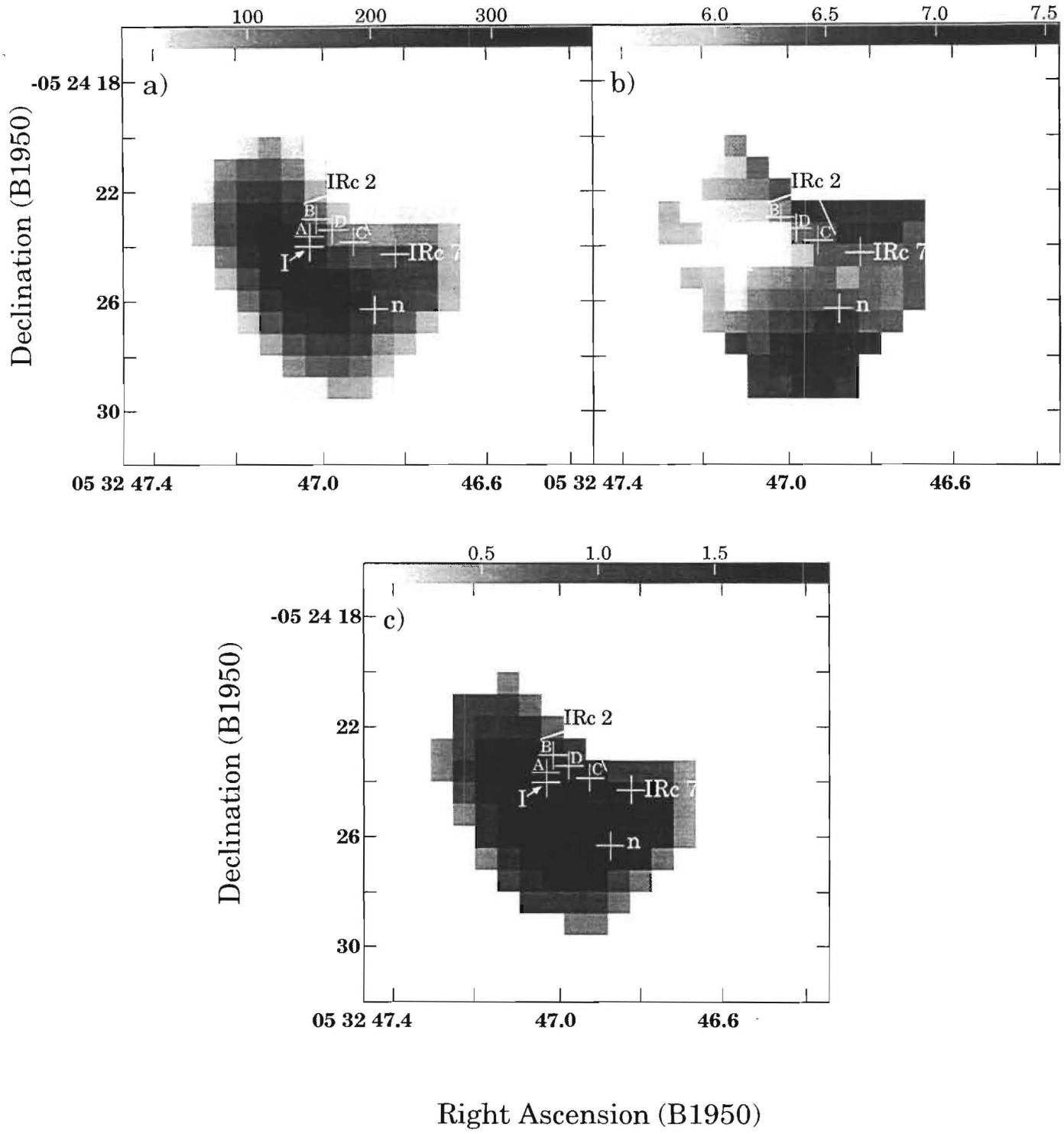
100
200
300
6.0
6.5
7.0
7.5
a)
b)
c)
-05 24 18
22
26
30
Declination (B1950)
IRc 2
B
A
D
C
I
IRc 7
n
05 32 47.4
47.0
46.6
0.5
1.0
1.5
Right Ascension (B1950)

Fig. 3

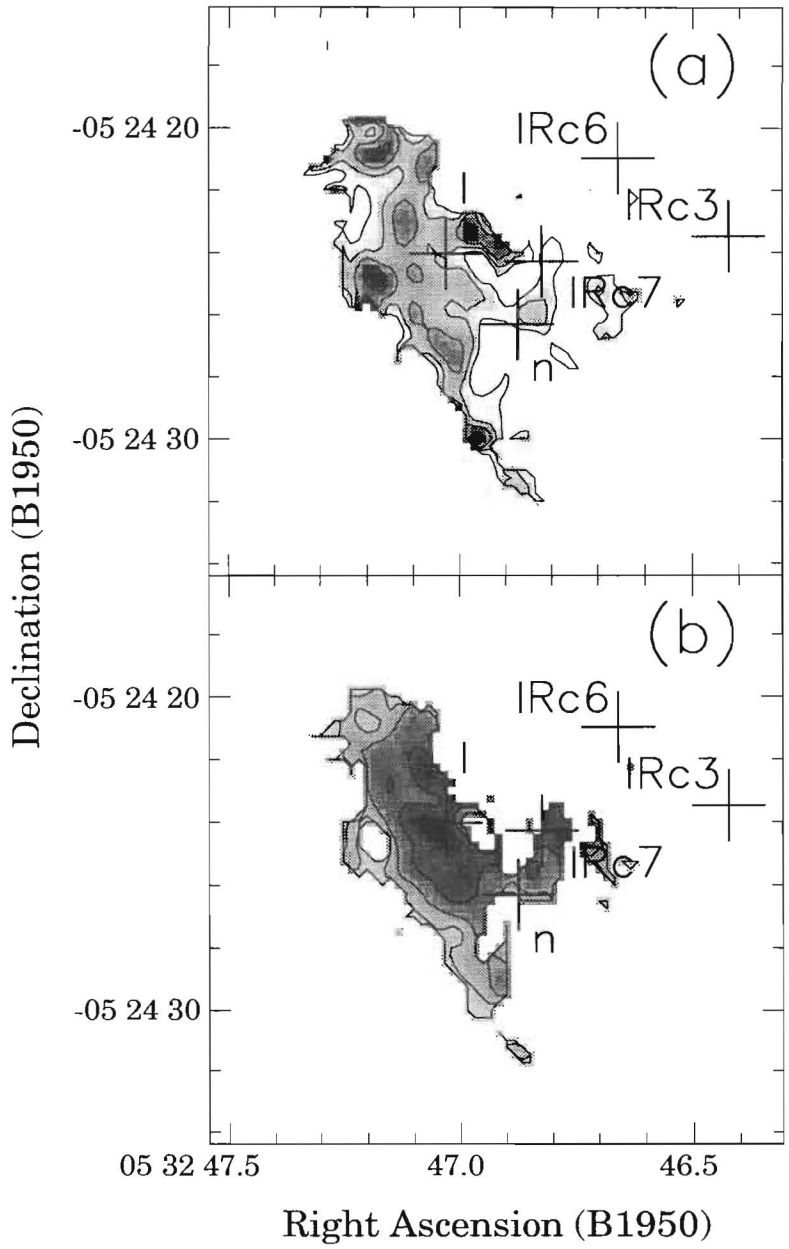
(a)
IRc6
IRc3
IRc7
l
n
(b)
IRc6
IRc3
IRc7
l
n
-05 24 20
-05 24 30
-05 24 20
-05 24 30
Declination (B1950)
05 32 47.5
47.0
46.5
Right Ascension (B1950)

Fig. 4

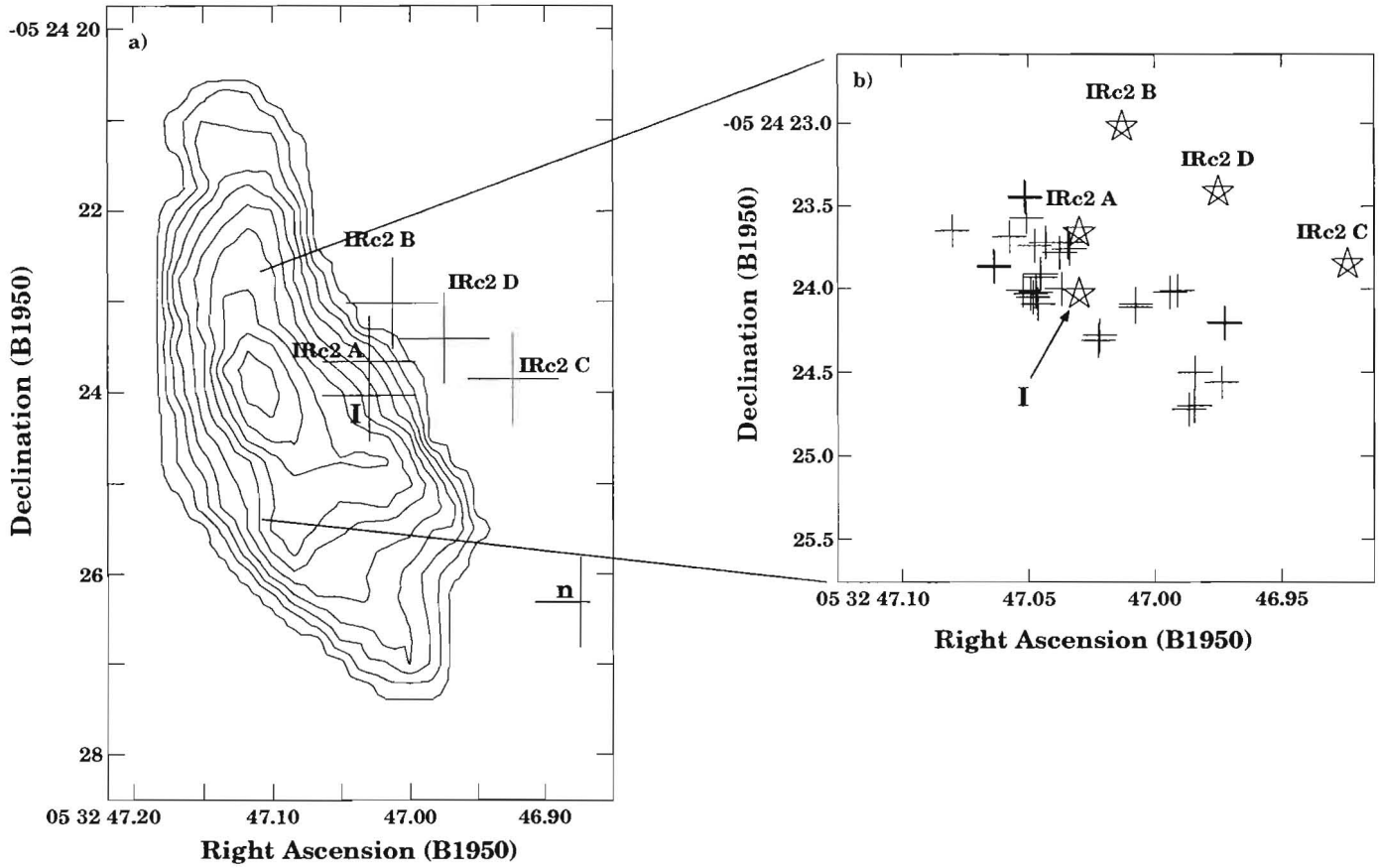
a)
-05 24 20
22
24
26
28
Declination (B1950)
IRc2 B
IRc2 D
IRc2 A
IRc2 C
I
n
05 32 47.20
47.10
47.00
46.90
Right Ascension (B1950)
b)
IRc2 B
IRc2 D
IRc2 A
IRc2 C
I
-05 24 23.0
23.5
24.0
24.5
25.0
25.5
Declination (B1950)
05 32 47.10
47.05
47.00
46.95
Right Ascension (B1950)

Fig. 5

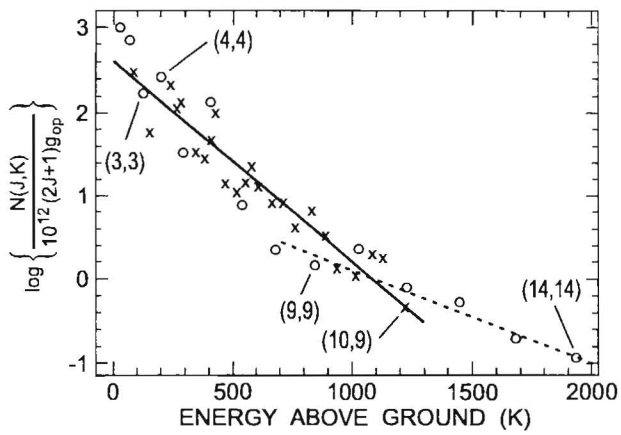
(4,4)
(3,3)
(9,9)
(10,9)
(14,14)
3
2
1
0
-1
0
500
1000
1500
2000
ENERGY ABOVE GROUND (K)
log { N(J,K) / 10^12 (2J+1)g_op }

Fig. 6